The vortices of homogeneous geostrophic turbulence

By JAMES C. McWILLIAMS[1], JEFFREY B. WEISS[2]
AND IRAD YAVNEH[3]

[1]Department of Atmospheric Sciences and Institute of Geophysics and Planetary Physics, UCLA,
Los Angeles, CA 90095-1565, USA
[2]Program in Atmospheric and Oceanic Science, University of Colorado,
Boulder, CO 80309-0391, USA
[3]Department of Computer Science, The Technion, Haifa 32000, Israel

A coherent-vortex analysis is made of a computational solution for the free decay of homogeneous, Charney-isotropic geostrophic turbulence at large Reynolds number. The method of analysis is a vortex detection and measurement algorithm that we call a vortex census. The census demonstrates how, through non-conservative interactions among closely approaching vortices, the vortex population evolves towards fewer, larger, sparser, and more weakly deformed vortices. After emergence from random initial conditions and a further period of population adjustment, there is a period of approximately self-similar temporal evolution in the vortex statistics. This behaviour is consistent with a mean-vortex scaling theory based on the conservation of energy, vortex extremum, and vortex aspect ratio. This period terminates as the population approaches a late-time non-turbulent end-state vortex configuration. The end state develops out of merger and alignment interactions among like-sign vortices, and even during the scaling regime, local clusters of nearly aligned vortices are common.

1. Introduction

Geostrophic turbulence is the name given to the nonlinear advective dynamics of rapidly rotating, strongly stably stratified fluids. It is thus an important process for large-scale winds and currents on Earth whose Rossby and Froude numbers are small:

$$Ro = \frac{V}{fL} \ll 1, \qquad Fr = \frac{V}{NH} \ll 1, \tag{1}$$

where V is a characteristic horizontal velocity, f is the Coriolis frequency for the Earth's rotation, N is the buoyancy frequency for the mean density stratification, L is a typical horizontal length scale, and H is a vertical scale (the vertical direction is parallel to gravity). For small Ro and Fr, the equations of fluid dynamics asymptotically simplify to the quasi-geostrophic equations (QG),

$$\frac{D\tilde{q}}{Dt} = \mathcal{NCT}. \tag{2}$$

Here

$$\tilde{q} = f + \nabla_h^2 \psi + \left(\frac{b}{N^2}\right)_z \tag{3}$$

is the QG potential vorticity; h denotes the horizontal component of a vector; ψ is the streamfunction for the horizontal velocity,

$$\boldsymbol{u}_h = \hat{z} \times \boldsymbol{\nabla}_h \psi; \tag{4}$$

$$b \equiv g(1 - \rho/\rho_o) = f\psi_z \tag{5}$$

is the buoyancy (i.e. normalized density fluctuation away from the mean stratification);

$$\frac{\mathrm{D}}{\mathrm{D}t} = \partial_t + \boldsymbol{u}_h \cdot \boldsymbol{\nabla}_h \tag{6}$$

is the substantial derivative with only horizontal advection; and $\mathscr{NCT}$ denotes forcing, diffusion, and any other non-conservative effects. Because we shall restrict this paper to the f-plane (i.e. constant f), we only need to consider the potential vorticity deviation, $q = \tilde{q} - f$.

Charney (1971) presents the founding theoretical analysis of geostrophic turbulence, and Herring (1980) assesses, and largely confirms, Charney's conjectures by using closure-theory calculations of (2)–(6). These analyses assume spatial homogeneity in all three directions. This situation is the most highly idealized formulation of geostrophic turbulence that manifests its essential advective dynamics. Therefore, the behaviour in homogeneous geostrophic turbulence is an important paradigm for theoretical geophysical fluid dynamics. However, spatial homogeneity is not geophysically realistic because of boundaries and spatial variations in f and N. Furthermore, the atmosphere and ocean are both thin fluid layers, whose aspect ratio is too small for motions with large geographical extent to be consistent with Charney's analysis. For these reasons there have been many subsequent theoretical and computational studies of geostrophic turbulence that have been either inhomogeneous in one or more of these ways or else anisotropic in the sense of deviating from the particular form of isotropy defined below (e.g. Rhines 1979; Salmon 1982; Hua & Haidvogel 1986; McWilliams 1989; Metais, Riley & Lesieur 1994; Metais *et al.* 1996; Hua, McWilliams & Klein 1998; Dritschel, de la Torre Juárez & Ambaum 1999). Nevertheless, in spite of the anisotropic influences in nature, there is observational support for Charney's prediction about the shape of the wavenumber spectrum, in both the atmosphere (Boer & Shepherd 1983; Nastrom & Gage 1985) and the ocean (Fu 1983; Stammer 1997).

The only prior computational study that is spatially homogeneous and appropriately isotropic is McWilliams, Weiss & Yavneh (1994, hereafter referred to as MWY94). (See Appendix A for its posing and numerical methods, and a summary of the evolutionary behaviour of its statistical moments and wavenumber spectra; also see Clyne, Scheitlin & Weiss (1998) for additional visualizations.) This solution, too, largely confirms the cascade behaviours conjectured by Charney. There is approximate conservation of total energy,

$$\mathscr{E} = \frac{1}{2} \iiint (\boldsymbol{u}_h^2 + b^2/N^2)\,\mathrm{d}\mathscr{V}.$$

In the absence of forcing and as the Reynolds number, *Re*, becomes large, $\mathscr{E}$ is transferred primarily towards larger scales in an *inverse cascade*. In contrast, there is substantial dissipation of the potential enstrophy,

$$\mathscr{Z} = \iiint q^2\,\mathrm{d}\mathscr{V},$$

within a finite time at any finite *Re*, and $\mathscr{Z}$ is transfered primarily towards smaller

scales in a *forward cascade*. Both of these cascades occur in all three spatial dimensions. Furthermore, there is the possibility of isotropy in the spatial structure of ψ and q with respect to a vertically stretched coordinate frame $(x, y, Nz/f)$, which we call *Charney isotropy*. In this frame, the relationship between streamfunction and potential vorticity simplifies to

$$q = \nabla^2 \psi, \qquad (7)$$

where ∇ is the three-dimensional isotropic gradient operator. MWY94 demonstrates that Charney isotropy is approximately established and maintained by the geostrophic turbulent cascades, in spite of the extreme anisotropy of the advection in (2) and (6). However, there are modest but significant departures from Charney isotropy: based on analysis of anisotropy in the wavenumber spectrum MWY94 shows that flow structures in the $\psi(x, y, z)$ field are relatively tall (i.e. with $NH/fL > 1$) on scales larger than the peak of the energy spectrum, slightly short over a broad range of intermediate scales, and quite short in the dissipation range at very small scales. The first of these departures from Charney isotropy may be due to the intrinsic anisotropy of QG at infinite length scales; the barotropic component, $\overline{\psi}^z(x_h, t)$, has a meaningful velocity field and advective evolution in (2), whereas the complementary component, $\overline{\psi}^{x_h}(z, t)$, has no advective evolution in (2) and thus can be absorbed into the mean stratification by (5). The MWY94 solution has finite periodicity lengths, hence finite wavenumber discretization, and its barotropic component grows with time at the largest available horizontal scales in the domain. This late-time growth of the barotropic component is also seen in the other computational studies of geostrophic turbulence cited above, especially where the domain aspect ratio is too small for Charney isotropy in the largest-scale baroclinic motions.

The MWY94 solution also shows the development of substantial intermittency associated with the emergence of coherent vortices, as are also found in nature and in computational solutions for many different regimes of turbulence. In freely decaying, homogeneous geostrophic turbulence, the elemental coherent vortices are compact, monopolar regions of large q (figures 1–3). Since advective dynamics is parity symmetric in QG (i.e. the transformation $(\psi, q, x, y) \leftrightarrow (-\psi, -q, x, -y)$ leaves (2)–(3) unaltered), vortices of both signs behave the same and are equally likely to develop from the random initial conditions. The vortices are approximately Charney-isotropic, which is evident from the approximately spherical shapes in figures 1–2. As the turbulence evolves with respect to its bulk statistical measures (e.g. energy and enstrophy cascades, and dissipation), so too does the vortex population. There are trends towards fewer, larger, sparser vortices. At very late times, when the inverse cascade has transferred substantial energy to the domain scale, the elemental vortices tend to aggregate into two columns with different signs (figure 3). These vortex aggregation behaviours are necessarily related to inverse energy cascade and growth of the barotropic component on large horizontal scales. The aggregation processes are horizontal merger and vertical alignment of proximate, like-sign vortices (Verron, Hopfinger & McWilliams 1990; Polvani 1991; Viera 1995; Sutyrin, McWilliams & Saravanan 1998; von Hardenberg *et al.* 1999).

The purpose of the present paper is to report on a vortex-based statistical analysis of the MWY94 solution. This is a useful alternative to more familiar statistical descriptors (e.g. moments and spectra) in a situation where the vortex organization is strong (figures 1–3). Another motivation comes from the hypothesis that geostrophic turbulence is controlled by the self-, pair-, and collective-dynamics of its coherent vortices. Perhaps the most direct way to demonstrate the validity of this hypothesis
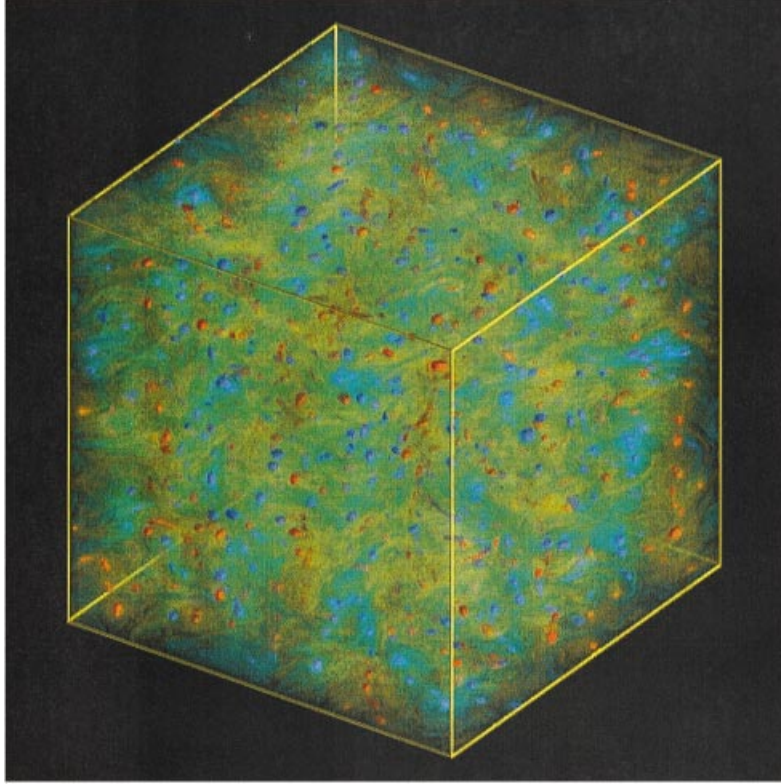
FIGURE 1. Potential vorticity, $q(x, y, z)$, in the MWY94 solution at $t = 5.0$, shortly after vortex emergence. Greens and blues indicate progressively more positive q, while yellows and oranges indicate progressively more negative negative q. Locations with $|q|/\max[|q|] < 3\%$ are completely transparent and not visualized. Locations with $3\% < |q|/\max[|q|] < 37\%$ are partially transparent and seen as hazy regions. Locations with with $|q|/\max[|q|] > 37\%$ are opaque and seen as solid surfaces. For more details about the visualization technique see Clyne *et al.* (1998).

would be to construct a skillful vortex-based dynamical system. This has been done for some behaviours in two-dimensional turbulence (i.e. monopolar vortices: Carnevale *et al.* 1991; Benzi *et al.* 1992; Weiss & McWilliams 1993; Riccardi, Piva & Benzi 1995), three-dimensional turbulence (i.e. vortex filaments: Chorin 1994), and thermal convection (i.e. plumes: Arakawa & Schubert 1974). No such theory has yet been developed for geostrophic turbulence, and here we take the preparatory step of describing the structure and evolution of its vortex population in relation to what we believe are the important dynamical processes. Although we analyse only a single solution, we believe its qualitative characteristics are representative of freely decaying geostrophic turbulence (see Appendix A).

Our methodology for this is a vortex census algorithm that identifies the vortices in the solution and measures their size, strength, and shape. This algorithm is adapted

FIGURE 2. Potential vorticity, $q(x, y, z)$, in the MWY94 solution at $t = 25.6$, during the period of approximately scaling behaviour in the vortex population statistics. The format is the same as in figure 1.

FIGURE 3. Potential vorticity, $q(x, y, z)$, in the MWY94 solution at $t = 72.16$, as the non-turbulent end-state vortex configuration is being approached. The format is the same as in figure 1.
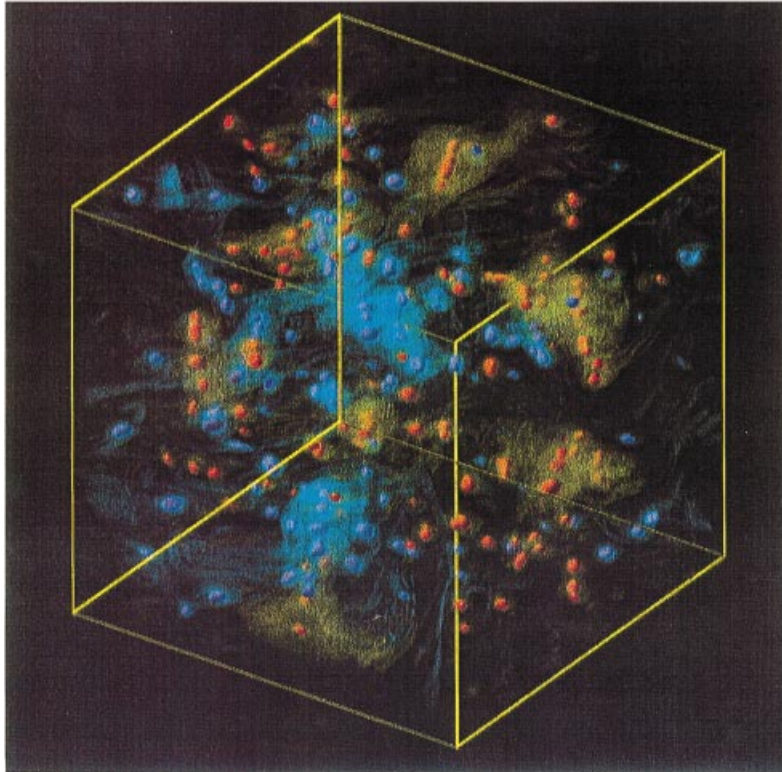
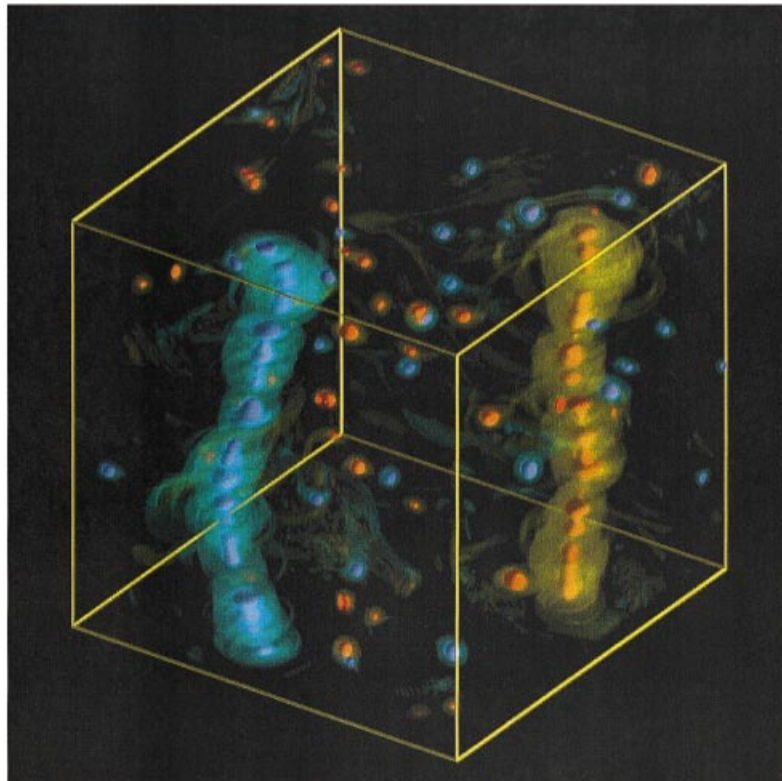FIGURE 2. For caption see facing page.

FIGURE 3. For caption see facing page.

from one previously applied to both two-dimensional and inhomogeneous geostrophic turbulence solutions (McWilliams 1990*a*, *b*). The reason for re-examining the vortices of geostrophic turbulence is that the MWY94 solution is appreciably different from and better than the one previously analysed (McWilliams 1989) in several ways: its resolution is finer (so *Re* is larger); it lacks vertical solid boundaries (and thus is homogeneous); and, most importantly, both its formulation and initial conditions are Charney-isotropic (see Appendix A).

2. A vortex census algorithm

Given adequate flow visualization, a coherent structure is readily perceptible through the human adeptness at pattern recognition. Nevertheless, we need a computational algorithm to quantify its detection and measurement. The simplest detection algorithm is a threshold in vorticity amplitude, whereby all large values are associated with coherent vortices (e.g. Benzi, Paternello & Santangelo 1986; Ohkitani 1991; Borue 1994). Although this often is in accord with the human perception, it gives an incorrect detection both before vortex emergence from complex initial conditions or forcing and when vorticity filaments detach during vortex interactions before they become weakened through dissipation. A more dynamically sophisticated possibility is the identification of vortices with regions having distinctive eigenvalues for either the velocity-gradient tensor (Weiss 1991; Jeong & Hussain 1995) or the Lagrangian acceleration-gradient tensor (Hua & Klein 1998; Hua *et al.* 1998), although these methods have not yet been implemented in practice. Another alternative is wavelet filtering, which has both an orderly mathematical framework and many successes in image processing and pattern recognition. This algorithm has successfully been applied to the vortices of two-dimensional turbulence by Farge & Philipovitch (1993) and Siegel & Weiss (1997). Nevertheless, based on our satisfactory previous experience, we choose to use a slightly modified form of the algorithm in McWilliams (1990*a*, *b*) that mimics aspects of the human perception criteria. We make no further comparisons here among alternative detection algorithms.

An ideal coherent vortex in geostrophic turbulence (figures 1–2) is axisymmetric and monotonically decreases in q in any horizontal plane with the distance r from its central extremum. These horizontal extrema lie along the same vertical line – the *axis* – at all vertical levels. Any such $q(r, z)$ configuration has $J(\psi, q) = 0$ and thus is a stationary solution of the inviscid QG equations, (2) with $\mathcal{NGF} = 0$. Furthermore, if such a q also is of only one sign within the vortex, then this stationary solution is demonstrably stable with respect to small perturbations by a Rayleigh integral condition. There are occasions when q of opposite sign lies in an annulus outside the vortex core (i.e. a shielded vortex). This allows for a possible barotropic instability. In our solutions, though, such annular configurations are rare, with at most weak q amplitude in the outer annulus. Also, they are usually non-persistent because the outer annulus is often stripped away during close interactions with other vortices. Weak q values in an outer annulus imply either vortex stability or at most a weak instability, depending upon the particular $q(r)$ profile. It is not uncommon, however, for there to be multiple q extrema of the same sign along a vortex axis (i.e. $q(r = 0, z)$ is single signed and has multiple extrema).

We define an elemental coherent structure – a *vortex element* – as a vorticity distribution that monotonically decays in z as well as r from its three-dimensional q extremum. A vortex element is thus a three-dimensional q-monopole, and the MWY94 solution demonstrates that it is by far the most common type of coherent vortex in

homogeneous geostrophic turbulence. We use the term *compound vortex* to denote a string of same-sign vortex elements connected along the axis by relatively strong q values, and we use the term *vortex cluster* to denote a group of same-sign vortices that are at least approximately aligned vertically but with intervening gaps having quite weak q values. The processes of vortex merger and axisymmetrization lead to the vortex elements approaching an ideal horizontal shape, and the process of alignment causes vortex elements to amalgamate into compound vortices and clusters. Clyne *et al.* (1998) demonstrates that the organization into vortex clusters sometimes can be reversed, and the clusters can separate into independent vortex elements, although some dissipation is involved and the process is thus not reversible in a thermodynamic sense. Opposite-sign (i.e. dipolar) axisymmetric vortices (i.e. with a common vertical axis) often exhibit baroclinic instability; however, with a small horizontal displacement between their axes they can be stable and propagate horizontally (NB the latter configuration is called a heton, or a modon when the dominant extrema are at the same level). These opposite-sign vortex pairings occur in the MWY94 solution only rarely and briefly. Finally, figure 3 suggests that the solution is asymptotically approaching an end-state configuration, with two opposite-sign, well-separated clusters of vortex elements and compound vortices, as a consequence of a long sequence of close interactions that result in mergers and alignments. Such a configuration is likely to be a stable stationary state if $\mathcal{NCT} = 0$, and if so any further evolution would be non-turbulent.

In a turbulent fluid full of vortices and other structures in q, the ideal shape almost never occurs because of mutual deformation by the shear in the velocity fields associated with the vortices. These deformations are small when the vortices dominate the q pattern and are well separated from each other. The vortex census algorithm interrogates the $q(x, y, z)$ field at a fixed time by comparing each location with the ideal vortex structure, and it identifies the regions where there is a close enough correspondence to declare that a vortex has been detected. The census also measures the properties of individual detected vortices. (In §5 we present a cluster analysis based on the population of detected vortices.)

The census algorithm has the following steps:

1. *Extrema*: Identify all three-dimensional extrema in q above a minimum amplitude, q_1, and spatially separated from any stronger extremum of the same sign by a minimum number, N_1, of non-extremum grid points in between. For the present solution we choose $q_1 = 10.0$ and $N_1 = 2$; these values are much smaller than the typical vortex extrema and sizes. With different initial conditions, q_1 should be adjusted proportionally to the typical vortex extrema; however, by specifying N_1 as a grid number rather than a physical length, it need not be adjusted with grid resolution.

2. *Axes*: Identify the axes associated with all three-dimensional extrema, defined as the line connecting horizontal extrema at adjacent levels as long as the horizontal shift between adjacent levels is less than N_2 grid points and the horizontal extremum exceeds a fraction, f_2, of the associated three-dimensional extremum. We choose $N_2 = 2$ and $f_2 = 0.2$. In addition, a check is made on whether three-dimensional extrema have intersecting axes. If so, then the weaker extremum is either discarded as an independent extremum but attached to the stronger extremum's axis or, if the weakest connecting q value along the axis is weaker than f_2 times the stronger extremum, then both three-dimensional extrema are retained but their axes are terminated at the point of weakest connecting q. With such a severed axis, the two vortices are members of a vortex cluster.

3. *Vortex elements*: Identify all distinct q extrema along an axis and the associated

weakest q amplitude on the axis segments connecting them. If the weakest amplitude value is weaker than the fraction f_3 times the weaker of the neighbouring extrema, then that location is defined as the boundary between axis segments associated with neighbouring vortex elements. Otherwise, the weaker of the two extrema is absorbed into the vortex element containing the stronger extremum. We choose $f_3 = 0.8$. If two vortex elements have a connecting q value along the axis whose relative amplitude lies in the range $[f_2, f_3]$, then they are parts of a compound vortex.

4. *Planar sets*:   In the horizontal plane through each vortex-element extremum, q_{ve}, we identify the set of connected grid points where $q/q_{ve} \geqslant f_4$. If the set contains a stronger horizontal extremum than q_{ve} or if the planar set is not simply connected, this vortex element is discarded as not independent. We choose $f_4 = 0.2$. (For a more detailed description of how the set is identified, see McWilliams 1990*a*.)

5. *Measures*:   For each vortex element we calculate the following measures of its structure. The *amplitude* is the absolute value of the three-dimensional extremum in q, q_{ve}. The half-*height*, h, is the average of the vertical distances between a vortex-element extremum and the upper and lower ends of its axis segment. The *tilt* away from vertical alignment, T, is the sum along a vortex-element axis segment of the horizontal displacement distances between adjacent levels divided by the vertical span of the axis segment. T can become quite large if the axis becomes tightly wound (e.g. as in a helix). The *area* of the planar set, A, is the number of grid points it contains times $\mathrm{d}s^2$ (where $\mathrm{d}s$ is the grid pacing). The *circumference* of the planar set, C, is the number of grid points on its periphery times $\mathrm{d}s$. The mean *radius* is $R = \sqrt{A/\pi}$. The *aspect ratio* is $a = h/R$. The *centroid displacement*, δ, of the planar set is the horizontal distance between the position of the vortex-element extremum and the first-order x and y moments of the q field (e.g. $\Sigma_{set} xq/\Sigma_{set} q$, etc., where Σ_{set} is the sum over all the grid points in the set). The *ellipticity* of the planar set is $\epsilon = \sqrt{\lambda_1/\lambda_2 - 1} \geqslant 0$, where $\lambda_1 \geqslant \lambda_2 \geqslant 0$ are the eigenvalues of the 2×2 matrix of the second-order x and y moments of the q field (e.g. $\Sigma_{set} x^2 q/\Sigma_{set} q$, etc.). The *circulation* of the planar set is $\Gamma = \Sigma_{set} q\mathrm{d}s^2$, and the planar-set *enstrophy* is $Z = \Sigma_{set} q^2\mathrm{d}s^2$.

6. *Detection criteria*:   For a candidate vortex element to be detected, it must also meet the following criteria related to the planar set:

$$\frac{R}{\mathrm{d}s} \geqslant D_R, \quad \frac{C}{2\pi R} \leqslant D_C, \quad \frac{\delta}{R} \leqslant D_\delta, \quad \epsilon \leqslant D_\epsilon. \tag{8}$$

These conditions are requirements that the vortex element is large enough to be at least marginally computationally credible on the grid and that its horizontal distortion from the ideal shape is not excessive. We choose the values $D_R = 1.0$, $D_C = 1.75$, $D_\delta = 0.35$, and $D_\epsilon = 2.5$, based on our fairly extensive experience with the algorithm (see McWilliams 1990*a*, *b*). Except for times prior to vortex emergence, the detected vortex population varies only slightly when these parameters are varied within, say, $\pm 30\%$, because there are relatively few ambiguous structures in q. Note that we have not imposed a detection condition based on T, beyond that implicit in the axis search parameter N_2, because we did not have a clear prior expectation of its distribution in the vortex population.

Our standard procedure is to perform this census on the full spatial domain. Because for large computational grids, such as ours, there are so many q extrema which pass the first step in the detection algorithm, the computational burden can be excessive. To escape this burden, we can perform the census only over a sub-domain. The algorithm is the same as above, except that we restrict the detection to compound vortices whose central extremum lies within the sub-domain, even if their associated

axes, vortex elements, and planar sets extend outside it. For comparison with census results over the full domain, we rescale all extrinsic quantities by the inverse of the sub-domain volume fraction (e.g. the compound vortex population size, n_{cv}), while intrinsic quantities do not need to be rescaled (e.g. the population-averaged radius, $\langle R \rangle$, where angle brackets denote an average over all the detected vortex elements). For the MWY94 solution, we do a full-domain census for $9.2 \leqslant t \leqslant 72.1$ and a sub-domain census for $2.8 \leqslant t \leqslant 9.2$. We start the census only at $t = 2.8$, since the size of the computation is quite large before then. For very early times (i.e. $t \leqslant O(1)$), the vortices have not yet become well enough organized from the random initial conditions for a census to be reliable. In practice, the sampling errors introduced by a sub-domain census do not seem excessive, as can be judged from the figures below near where the two sampling procedures overlap. Since the census calculation makes use of data from only a single time, a general indication of its sampling errors comes from the size of the incoherent temporal fluctuations in its population-mean estimates. These errors also are modest compared to the evolutionary trends in the vortex statistics that are our primary focus.

In summary, the census measures the properties of the vortex population at a given instant in time. The census counts the number of extrema in the vorticity field n_e, the number of those extrema which qualify as coherent vortex elements n_{ve}, and the number of resulting compound vortices n_{cv}. Each vortex element is described by its position, amplitude q_{ve}, planar area A, planar circumference C, planar radius R, planar ellipticity ϵ, planar circulation Γ, planar enstrophy Z, half-height h, and axial tilt T.

3. The census report

We perform the census for 41 times between $t = 2.8$ and 72.1, with both full- and sub-domain calculations at the transition time, $t = 9.2$. The times are distributed with an approximately exponentially increasing spacing, since the evolution of most statistical measures of turbulence has an approximately power-law dependence on time. Such temporal scaling behaviour and its implied self-similar statistical evolution are obviously of great theoretical interest here (as they also have been for two-dimensional turbulence). This hypothesis is difficult to test unambiguously, even with the rather large size of the MWY94 solution. To do so would require a larger value for the initial spectrum-peak wavenumber, κ_0, in order to have a larger n_{ve} at the time of vortex emergence. A larger κ_0 would imply a smaller effective Re for the vortex evolution, unless the computational grid size were also increased, which was infeasible. Nevertheless, we plot many of our census results logarithmically against time and summarize their forms through approximate power-law fits (see table 1 for estimates of the temporal exponents). The results are strongly suggestive of approximate temporal scaling behaviour (e.g. for the vortex population shown in figure 2) beginning well after the time of vortex emergence (e.g. figure 1) and stopping well before reaching the non-turbulent end state (e.g. figure 3).

After the initial period of emergence ($t < 2$), the population size decreases with time. This trend has several causes. Existing vortices disappear both by vortex amalgamation through merger and alignment and by vortex destruction through straining deformations. Also, new vortices emerge only rarely from the background (i.e. non-vortex) component of the q field at later times. This evolution is shown in figure 4, for both the number of three-dimensional extrema, $n_e(t)$, found in step 1 of the census algorithm, and the number of compound vortices, $n_{cv}(t)$, detected in step 6.

Quantity	Fit	Scaling $L_v \sim n_v^{-1/3}$	Theory $L_v \sim R_v$
n_{cv}	-1.25 ± 0.10	-1.25	-1.25
$\langle q_{ve} \rangle$	$+0.02 \pm 0.07$	0.0	0.0
$\langle a \rangle$	-0.03 ± 0.05	0.0	0.0
$\mathscr{E}$	-0.003 ± 0.001	0.0	0.0
$\langle \Gamma \rangle$	$+0.45 \pm 0.10$	$+0.55$	$+0.50$
$\langle Z \rangle$	$+0.34 \pm 0.10$	$+0.55$	$+0.50$
$\langle R \rangle$	$+0.29 \pm 0.05$	$+0.28$	$+0.25$
$\langle h \rangle$	$+0.28 \pm 0.05$	$+0.28$	$+0.25$
$\mathscr{Z}$	-1.0 ± 0.2	-0.42	-0.50
$\langle D \rangle_{\pm}$	$+0.43 \pm 0.05$	$+0.42$	$+0.42$

TABLE 1. Power-law exponents. The fitted values for the exponents are averages of estimates for several different intervals during the period $10 \leqslant t \leqslant 70$; their uncertainties represent the spread of these estimates, which is larger than the standard error of any given fit. The scaling theory exponent for n_{cv} is determined directly from the solution fit.

The ratio between them, n_e/n_{cv}, decreases with time, indicating an increasing degree of organization of the turbulence into well formed vortices. The functional form for $n_{cv}(t)$ roughly matches a power law, $\sim t^{-\gamma}$ with $\gamma \approx 1.25 \pm 0.10$, at intermediate times well after vortex emergence and well before the approach to the non-turbulent end state. The error estimate here is dominated by the choices of the beginning and end times for the time interval within which to make the power-law fit. The differences between the fitted exponents due to the end-point choices are substantially larger than the standard error for the fit with any particular interval. This fitted value for γ is consistent with the QG census analysis in McWilliams (1990*b*), and it is significantly larger than the value found in a temporal scaling regime of two-dimensional turbulence, $\gamma \approx 0.725 \pm 0.025$ (Carnevale *et al.* 1991; Weiss & McWilliams 1993). We rationalize the larger γ of geostrophic turbulence as an indication of the increased opportunities for close approaches among vortices, hence for strong interactions that can decrease the population, in three dimensions compared to two.

Figure 5 shows the population size for both vortex elements and compound vortices, with $n_{ve}(t) \geqslant n_{cv}(t)$ by definition. A striking result is how close these two numbers are near the time of emergence, and how slowly they develop any appreciable difference. Even at the final time, corresponding to figure 3, their ratio is only 1.3. Thus, even after many close approaches, the alignment process yields relatively few compound vortices with well-distinguished multiple extrema along the vertical axis. Assuming that the alignment process is efficient, one would expect that the interaction of nearby same-sign vortices with small vertical separation would result in a single compound vortex composed of multiple vortex elements. Since q cannot be transferred between different levels by advection in (2) and (6), such a compound vortex would, in the inviscid case, last until disrupted by further vortex interactions. The scarcity of such compound vortices must thus be due to one of several possibilities: efficient blending of separate extrema on the axis by the vertical diffusion terms in (2) (see (A 1) in Appendix A); inefficient amalgamating due to a relatively small interaction cross-section for two vortices with $O(h, R)$ vertical separation between their extrema; or frequent severing of aligned compound vortices at their connecting weakest q value
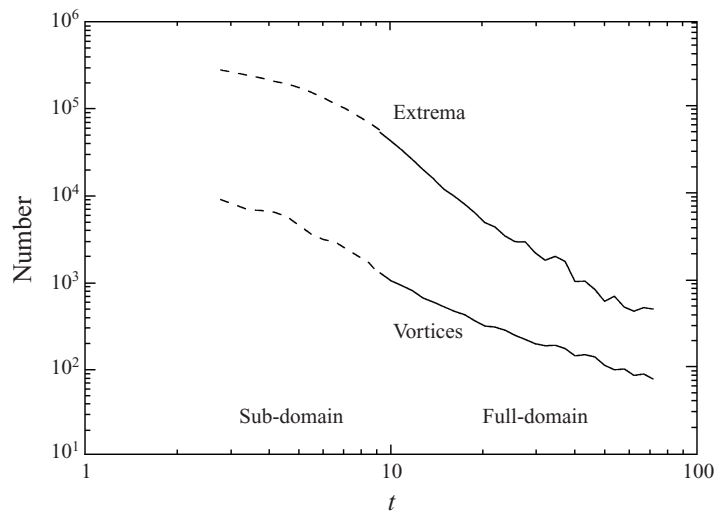
FIGURE 4. The number of extrema and compound vortices, $n_e(t)$ and $n_{cv}(t)$, from the vortex census.

through straining interactions with other vortices. A diffusion time on the vortex scale, h^2/v, is much larger than the solution times under consideration here. Diffusion can only be effective in blending vertical extrema if very sharp q gradients develop near the extrema along the axis during merger or alignment, but this would be inconsistent with the approximate preservation of q extremal values (see figure 6 below). So we conclude that diffusion is not the primary explanation. The pair-interaction study by Sutyrin *et al.* (1998) demonstrates a reduction in the tendency towards alignment for like-sign vortices with $O(R)$ vertical separation and smaller horizontal separation, compared to the tendency with both separations $O(R)$. So perhaps alignment interactions, even if frequent, are rarely carried to completion. Also, we see frequent and persistent same-sign, multi-vortex interactions in animations of $q(\boldsymbol{x}, t)$ (manifested in the clustering behaviour analysed in §5), and perhaps this also inhibits the completion of alignments or contributes to severing of compound vortices. Finally, in the inhomogeneous, Charney-anisotropic solution in McWilliams (1989) – where the vertical size of the domain is relatively small and the vertical grid resolution is coarse – there is a much greater abundance of compound vortices with multiple vortex elements than in the MWY94 solution.

Figure 6 shows the vortex amplitudes, both the strongest one, $\max[q_{ve}](t)$, and the population mean, $\langle q_{ve}\rangle(t)$. The strongest extremum has a steady decrease, cumulatively by about 50% over the duration of the analysis. This is quite small compared with the r.m.s. measure of the potential vorticity, $\mathscr{Z}^{1/2}$, that decreases by about 90% (see Appendix A). The scaling theory of two-dimensional turbulence is based on the assumption that the amplitude of a vortex extremum is preserved as long as the vortex survives (Carnevale *et al.* 1991), and we believe this assumption may also be appropriate for geostrophic turbulence as $Re \to \infty$ (see §4). The rationale is that the centre of a coherent vortex experiences little deformation, hence little strain-enhanced diffusion to weaken the extremum, as long as other vortices either remain distant or are sufficiently weaker in amplitude that close encounters do not disrupt the stronger vortex. Obviously, these conditions are not met precisely in the MWY94 solution, although the decrease in $\max[q_{ve}](t)$ here is somewhat smaller than
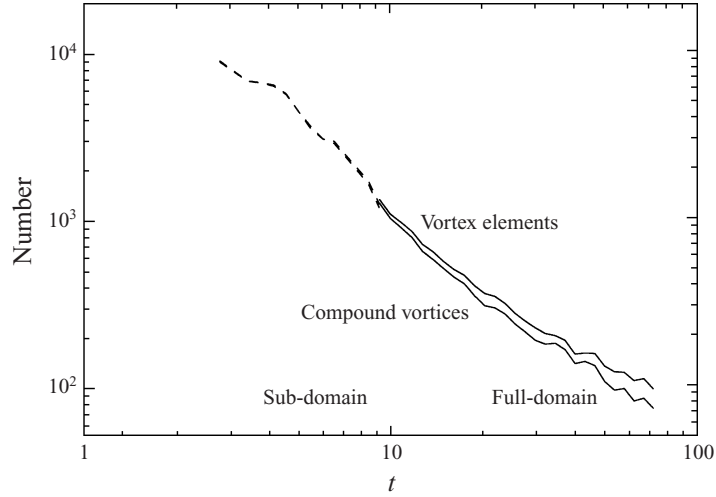
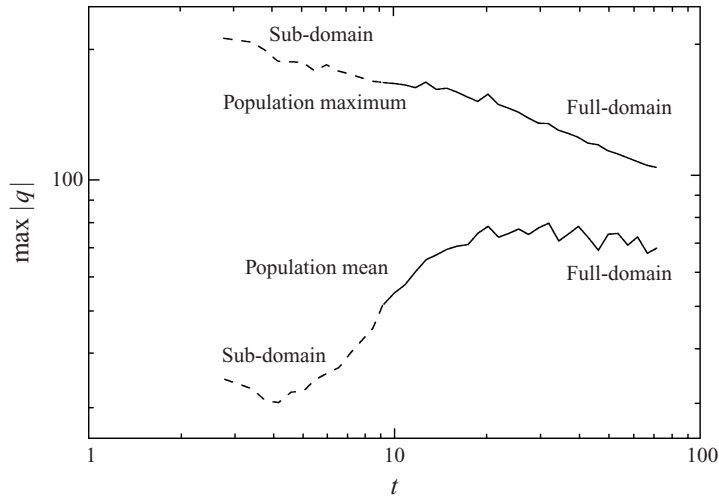FIGURE 5. The number of vortex elements and compound vortices, $n_{ve}(t)$ and $n_{cv}(t)$, from the vortex census.

FIGURE 6. The largest and population-mean vortex-element amplitude, $\max[q_{ve}](t)$ and $\langle q_{ve}\rangle(t)$, from the vortex census.

in the McWilliams (1989, 1990*b*) solution with its smaller *Re* value. In contrast, the population-mean amplitude, $\langle q_{ve}\rangle(t)$, has an initially small decrease near the end of the relatively dissipative emergence phase and then a steady increase for a lengthy time interval between $t \approx 4$ and $t \approx 15$. This growth behaviour is also seen in the McWilliams (1990*b*) analysis. Since an individual vortex amplitude should only decrease in (2) and (A 1) – at least for sufficiently smooth vortex profiles to avoid the anti-diffusive behaviour possible with hyperdiffusion – then an increasing $\langle q_{ve}\rangle(t)$ implies an evolution in the population distribution function for q_{ve} wherein the number of weak vortices declines more rapidly than the number of strong ones. This is consistent with the idea that pair interactions between unequal vortices deform the
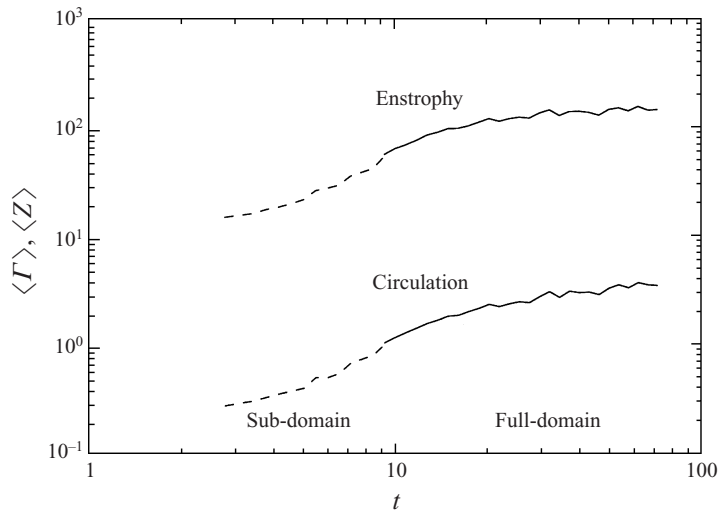
FIGURE 7. The population-mean vortex-element planar circulation and enstrophy,
$\langle \Gamma \rangle(t)$ and $\langle Z \rangle(t)$, from the vortex census.

weaker one more and cause it to disappear from the census count: the weaker vortex is either deposited within the profile of the stronger one by amalgamation or sheared out until diffusion further weakens it. After $t \approx 15$, there is little further evolution of $\langle q_{ve} \rangle(t)$; this is suggestive of a scaling regime with a self-similar population distribution function.

Figure 7 shows the evolution of the population-mean vortex-element planar circulation and enstrophy, $\langle \Gamma \rangle(t)$ and $\langle Z \rangle(t)$. They both are steadily increasing with time. Before $t \approx 15$, $\langle \Gamma \rangle(t)$ and $\langle Z \rangle(t)$ grow even more rapidly than afterwards. This is consistent with the interpretation, given to figure 6 above, that smaller, weaker vortices are experiencing a disproportionately high destruction rate through interactions with larger, stronger vortices during this phase of population adjustment. After $t \approx 15$, the functional forms are approximately power laws, $\sim t^{\alpha}$. We can fit $\langle \Gamma \rangle(t)$ with a value of $\alpha_{\Gamma} \approx 0.45 \pm 0.10$, while the value for $\langle Z \rangle(t)$ is smaller by perhaps 25% during the period after $t \approx 15$ (see table 1). Since these two quantities differ in their dependence on q inside the vortices, but not in their dependence on the planar area within a vortex, we deduce from the rough equivalence of their α values that changes in the vortex radius are the primary influence on their evolution. This is consistent with the interpretation that horizontal merger is an important evolutionary process here, since it conserves the q amplitude in the core of a participating vortex but increases its area. On the other hand, from the modest difference in the α values for $\langle \Gamma \rangle(t)$ and $\langle Z \rangle(t)$, we deduce that there is also some evolutionary change in the planar profile shapes for q in the same sense as diffusion (i.e. acting to decrease Z while preserving Γ). Hence, the vortex cores are not entirely free from dissipative influences in our solution. These values for α are close to the value in the temporal scaling regime for two-dimensional turbulence (i.e. where $\alpha_{\Gamma} \approx 0.38 \pm 0.02$; Weiss & McWilliams 1993), where horizontal merger is the dominant evolutionary process for vortices.

The growth in vortex size is evident in figure 8. The mean radius, $\langle R \rangle(t)$ grows more rapidly before $t \approx 15$ and more slowly afterwards, with an approximate power-law form at later times and an exponent $\alpha_R \approx 0.29 \pm 0.05$. This value is somewhat larger
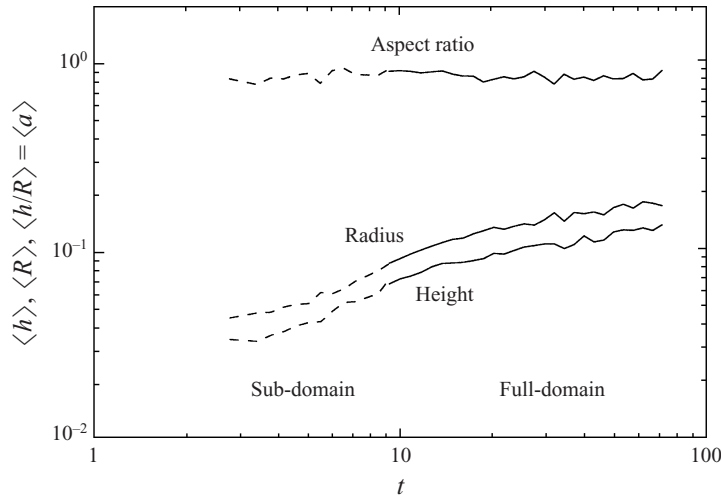
FIGURE 8. The population-mean vortex-element radius, $\langle R \rangle(t)$, half-height, $\langle h \rangle(t)$, and aspect ratio, $\langle a \rangle(t)$, from the vortex census.

than but not greatly inconsistent with either the value in the temporal scaling regime for two-dimensional turbulence (i.e. $\alpha_R \approx 0.19$) or with the interpretation given above for planar circulation and planar enstrophy increasing roughly $\sim \langle R \rangle^2$. Again we find support for the ideas of early-time population adjustment and the importance of the merger process.

Particularly striking in figure 8 is the near constancy of the population-mean vortex-element aspect ratio, $\langle a \rangle(t)$. The aspect ratio is constant throughout the time period where other quantities show approximately scaling behaviour, as well as before and after this period. Consistent with $\langle a \rangle$ constancy, $\langle h \rangle(t)$ has a systematic growth that closely matches that of $\langle R \rangle(t)$. In the stretched isotropic coordinates in which this solution is calculated (Appendix A), a value $a = 1.0$ corresponds to Charney isotropy for the vortex $q(r, z)$ profile. The measured value here is $\langle a \rangle \approx 0.83 \pm 0.03$. This indicates that the elemental vortices are somewhat flattened ellipsoids rather than Charney-isotropic spheres. This sense of deviation from isotropy is the same as seen in MWY94 in the spectrum for the intermediate wavenumber range between the energy peak and the dissipation range. The inhomogeneously and anisotropically posed problem in McWilliams (1989, 1990*b*) also has an approximate constancy of $\langle a \rangle(t)$, but at a much larger value of $\langle a \rangle \approx 1.5$. We interpret this difference as due to the difference in posing – in particular the influences of a small domain aspect ratio, solid vertical boundaries, and coarse vertical resolution on increasing the barotropic component of the flow.

The dynamical mechanism for $\langle a \rangle$ constancy is poorly known. One can argue generally that a values are limited from above and below by barotropic and baroclinic instability, respectively, although such instabilities are precluded for the particular profile shape of a q-monopole. One can argue that h can grow through alignment interactions, particularly those between vortex elements whose central extrema are vertically separated by a distance $O(h)$, but the absence of compound vortices with multiple vortex elements (figure 5) argues against this being a common process except perhaps for rather small vertical separations. Although h cannot grow by vertical advective fluxes with the QG operator (6), it can grow diffusively by (A 1) at a slow
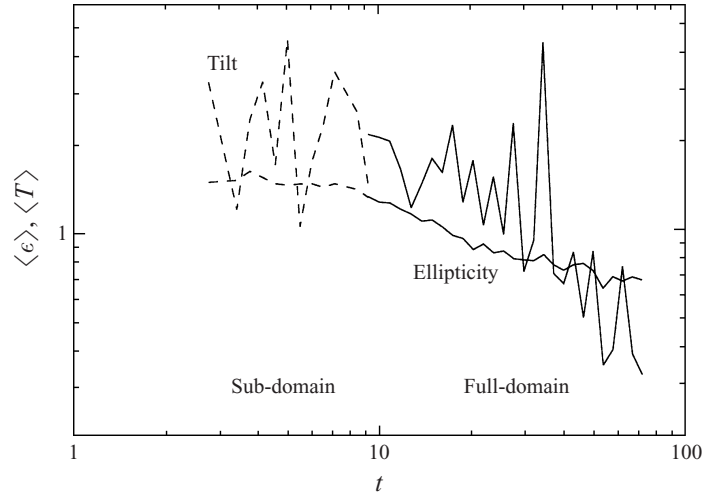
FIGURE 9. The population-mean vortex-element distortions from the vortex census: the planar ellipticity, $\langle \epsilon \rangle(t)$, and the vertical tilt, $\langle T \rangle(t)$.

rate of $v/h^2 = O(Re^{-1})$ for undisturbed vortices. Thus, there are several possible mechanisms for h growth, but none of them are yet known to have a strong selection for a constancy. Perhaps the most plausible hypothesis is that geostrophic vortices experiencing frequent episodes of deformation by a varying large-scale strain field relax dissipatively towards the ideal axisymmetric, aligned configuration in a way that strongly pushes its aspect ratio towards an a value somewhat less than unity. Of course, this hypothesis is in need of further proof.

The strain in the far field of a geostrophic vortex decreases $\sim d^{-3}$ where d is the distance from the vortex. The aggregate strain field of the vortex population is the cause of vortex deformations away from the ideal shape. The closest neighbouring vortices contribute the most to the strain field, and particularly close approaches cause particularly large deformations that lead to dissipation, merger, and alignment. Since the vortex population decreases with time (figure 4), the average separation between vortices increases. We estimate the average separation as $\overline{d} \sim 2\pi n_{ve}^{-1/3}$, hence the mean strain rate as $\sim n_{ve}^{-1}$. Thus, the average magnitudes of the strain field and resulting deformation should also decrease. The latter behaviour is shown in figure 9, with respect to deviations both from horizontal axisymmetry, $\langle \epsilon \rangle(t)$ and from vertical alignment, $\langle T \rangle(t)$. Both measures decrease with time as is qualitatively expected. Their values are $O(1)$, indicating that deviations from the ideal vortex shape are substantial except at very late times. Because of the evident curvature in their histories and the large temporal fluctuations in T, power-law fits to figure 9 are not well constrained. Nevertheless, we can conclude that the decay exponent is greater for T than for ϵ. The former is perhaps not greatly inconsistent with the decay exponent, γ, for n_{ve} and the mean strain rate, while the latter is clearly smaller.

4. A mean-vortex scaling theory for geostrophic turbulence

Encouraged, though not yet fully convinced, by the indications of scaling behaviour seen above, we can construct a simple scaling theory for a temporally self-similar evolution of the vortex population in geostrophic turbulence. It is based upon representing the fields in terms of a finite number, n_v, of coherent vortices, each with amplitude q_v,

radius R_v, and height h_v. For simplicity, we assume that all the vortices have the same values for these properties, i.e. we base the representation on a 'mean vortex'. Other vortex properties are constructed from these primary ones, e.g. $\Gamma_v \sim q_v R_v^2$, $Z_v \sim q_v^2 R_v^2$, etc.

Within this representation, we make the following assumptions about what is conserved in decaying geostrophic turbulence as $Re \rightarrow \infty$.

Energy: Using a Green's function representation for the solution of the three-dimensional Poisson equation in (7), we can write the total energy in terms of the potential vorticity as follows:

$$\mathscr{E} = \int \mathrm{d}\boldsymbol{x}_1 \int \mathrm{d}\boldsymbol{x}_2 \, q(\boldsymbol{x}_1) \, q(\boldsymbol{x}_2) \, G(\boldsymbol{x}_1, \boldsymbol{x}_2), \tag{9}$$

where $G \sim |\boldsymbol{x}_1 - \boldsymbol{x}_2|^{-1}$ in an infinite domain, with suitable corrections for the periodic domain of the MWY94 solution. Taking into account the partial cancellation among contributions to (9) from vortices of opposite sign, we can approximate the energy using our mean-vortex representation as

$$\mathscr{E} \sim n_v [q_v h_v R_v^2]^2 / L_v,$$

where L_v is a length scale. In the analogous scaling theory for two-dimensional turbulence, the energy depends on L_v in the form $\log(L_v)$, via the two-dimensional Green's function, and since logarithmic corrections are ignored in this scaling theory, no choice for L_v is required. Here $\mathscr{E} \sim 1/L_v$, and we must choose the length scale. There are two obvious choices based on scaling $\mathscr{E}$ as either the interaction energy for distant vortices, or as the self-energy for individual vortices. In the former case the appropriate length scale is the typical pair separation distance, $L_v \sim n_v^{-1/3}$, while in the latter case the appropriate length scale is the typical vortex size, $L_v \sim R_v$. We currently have no reason to choose one length scale over the over, and we present the scaling theory with both possible choices. (Interestingly, we shall see that the predictions are not quantitatively very different between these two choices.)

Vortex amplitude: q_v.

Vortex aspect ratio: $a_v \sim h_v / R_v$.

The first assumption of total energy conservation is well satisfied in the MWY94 solution with its large but finite Re (see Appendix A). The second assumption of q_v conservation is only approximately correct for this solution (e.g. see figure 6), and, because of our particular vortex representation of $\mathscr{E}$ above, the first assumption is also only approximately correct. These two assumptions are the same as in the temporal scaling theory for two-dimensional turbulence (Carnevale *et al.* 1991). The third assumption of constant aspect ratio is strongly supported by figure 8.

The final ingredient is the assumption that all statistical measures have power-law dependence on time. In particular, we assume that the population size decreases as

$$n_v(t) = n_v(t_0) \left(\frac{t}{t_0} \right)^{-\gamma} \sim t^{-\gamma} \tag{10}$$

for t_0 any time within the interval of scaling behaviour, with an empirically determined value for the exponent γ (e.g. $\gamma = 1.25$ from figure 5). We interpret the decreasing population size as the net of losses through merger and alignment and gains through new vortices emerging from q filaments outside vortices (although we have not yet seen many examples of the latter).

With these ingredients we can derive the temporal exponents for the other quantities.

Thus, the scaling theory predicts all exponents in relation to a single, empirically determined exponent, γ (i.e. the exponent for property μ is $\alpha_\mu = \alpha_\mu[\gamma]$). The exponent γ remains a parameter of the theory that is undetermined *a priori*. Assumed, fitted, and predicted values for the power-law exponents of various quantities are summarized in table 1. The size measures, h_v and R_v, have $\alpha_h = \alpha_R$ equal to either $2\gamma/9 = 0.28$ or $\gamma/5 = 0.25$, respectively, depending upon the choice of L_v in $\mathscr{E}$. These estimates are close to each other and they compare favourably with the empirical fits to figure 8. In addition, Γ_v and Z_v have exponents $\alpha_\Gamma = \alpha_Z = 2\alpha_R$, whose value is either 0.55 or 0.50. These values are somewhat larger than those from the fits to figure 7, indicating greater q dissipation within the surviving coherent vortices in the numerical solution than is assumed in the scaling theory.

As in the two-dimensional counterpart to this theory, we can make a mean-vortex estimate for the total potential enstrophy evolution, namely

$$\mathscr{Z} \sim n_v q_v^2 h_v R_v^2. \tag{11}$$

This yields a decay law of either $\sim t^{-\gamma/3}$ or $\sim t^{-2\gamma/5}$, respectively. The numerical value for this exponent is either -0.42 or -0.50, respectively, for $\gamma = 1.25$. In contrast, a power-law fit to $\mathscr{Z}(t)$ calculated from the MWY94 solution has an exponent of -1.0 ± 0.2, appreciably larger than that predicted by (11). This is a further indication that enstrophy dissipation is greater in the finite-*Re* numerical solution than in the infinite-*Re* scaling theory above. There is a similar discrepancy for the enstrophy decay exponent rate in two-dimensional turbulence (Weiss & McWilliams 1993).

5. Vertical alignment and clustering

In figure 3 we see a domain-scale ordering among the vortex positions that develops at late time. Here we present some quantitative measures of this collective behaviour.

The cause of the positional ordering is the strain-induced deformation among like-sign vortices that instigates the merger and alignment amalgamation processes. These processes are most familiar as pair interactions, so we begin with pair statistics. For each compound vortex we measure the distance to all other vortices and select the nearest neighbour. The distance is taken as the minimum over all separations between the vortex elements contained within each of the compound vortices. Because few vortices have multiple vortex elements except at late time (figure 5), the distinction between primary and secondary q extrema is not very significant. For each vortex i, we denote the minimum separation vector by $\boldsymbol{D}_i$, and minimum distance by $D_i = |\boldsymbol{D}_i|$. We also measure the absolute value of the angle of the minimum separation vector from the horizontal plane. Thus, if $\boldsymbol{D}_i = (X_i, Y_i, Z_i)$, then the angle is

$$\theta_i = \tan^{-1}\left[\frac{|Z_i|}{\sqrt{X_i^2 + Y_i^2}}\right]. \tag{12}$$

Figure 10 shows the population-mean, near-neighbour separation angles, $\langle\theta\rangle_\pm(t)$, distinguished by whether the nearest vortex has the same $(+)$ or opposite $(-)$ sign in q. At early time, $\langle\theta\rangle_\pm$ has a value close to the mean angle for a random vortex distribution, denoted by θ_0. Since an infinitesimal volume element $\mathrm{d}X\,\mathrm{d}Y\,\mathrm{d}Z$ is equal to $\mathscr{R}^2 \cos\theta\,\mathrm{d}\mathscr{R}\,\mathrm{d}\theta\,\mathrm{d}\phi$ in spherical coordinates, the most probable angle is

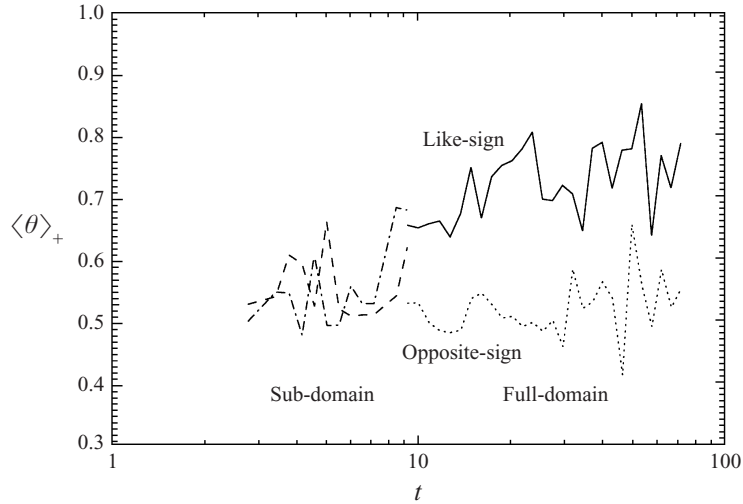$$\theta_0 = \int_0^{\pi/2} \theta\,\cos\theta\,\mathrm{d}\theta$$
$$= \pi/2 - 1. \tag{13}$$

FIGURE 10. The population-mean angles, $\langle\theta\rangle_{\pm}(t)$, relative to the horizontal plane, between pairs of nearest neighbour vortices, segregated by whether the pair is like-sign (dot-dash and solid lines) or opposite-sign (dashed and dotted lines) in the q extrema. The separation distance is measured between the nearest vortex-element extrema. The reference line at $\theta_0 = \pi/2 - 1$ is the value for a random orientation of separations.

Thus, there is no particular angular ordering as a result of the vortex emergence process. With further vortex evolution, $\langle\theta\rangle_+$ grows while $\langle\theta\rangle_-$ does not. This distinction begins to develop somewhere around $t = 7$, although it is difficult to be precise because of the large sampling error evident in figure 10 during the last part of the period in which sub-domain census sampling is used. Nevertheless, at late times a nearby like-sign vortex is much more likely to lie within a cone above or below its neighbour than to lie outside the cone. Mergers act to deplete nearby like-sign vortices outside the cone, and alignment acts to attract and retain nearby like-sign vortices within the cone. Since $\langle\theta_+\rangle$ remains well below $\pi/2$ even at late times, this indicates that alignment interactions usually do not proceed to completion. Furthermore, the vortex clusters support wave-like behaviour around the cluster axis which distorts the column from the vertical and makes $\theta_+ < \pi/2$ (Clyne *et al.* 1998). These waves are probably induced by variable straining from vortices outside the cluster, although once induced the waves are sustained by conservative interactions among the non-aligned vortices within the cluster (e.g. as in a QG point-vortex system).

The nearest opposite-sign vortices also have a persistent bias in their separation angle, such that $\langle\theta_-\rangle$ is slightly smaller than θ_0. This may be due to a baroclinic instability process that results when opposite-sign alignment occurs and the vertical shear is locally enhanced.

Figure 11 shows the the population-mean, near-neighbour separation distances, $\langle D\rangle_{\pm}(t)$, segregated by whether the nearest pair has the same $(+)$ or opposite sign $(-)$ for its q extrema. Here we see no significant difference between $\langle D\rangle_+$ and $\langle D\rangle_-$, neither after emergence nor with further evolution. Furthermore, both of $\langle D\rangle_{\pm}$ have a power-law (scaling) form, $\langle D\rangle \sim t^{\alpha}$, with $\alpha = 0.43 \pm 0.05$ after about $t = 10$. This value for α is very close to what results from the assumption that vortices are distributed in a volume-filling way, with $\langle D\rangle \sim n_{cv}^{-1/3}$; i.e. $\alpha = -\gamma/3 = 0.42$ for $\gamma = 1.25$ from figure 4. The actual values for $\langle D\rangle$ in figure 11 are only about one-quarter as large
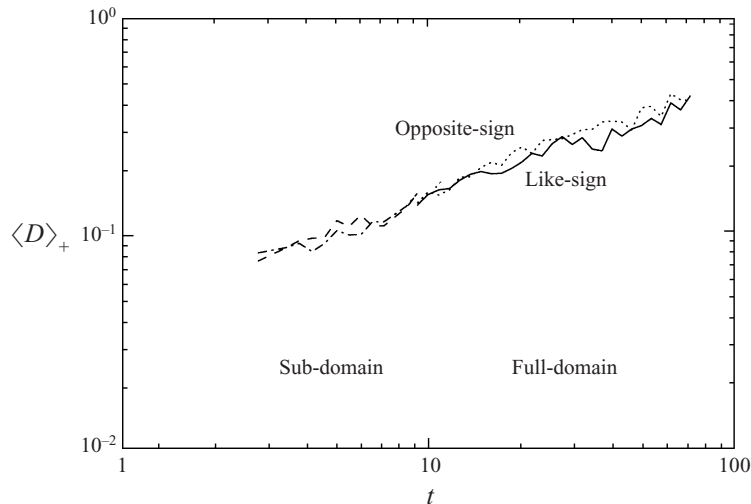
FIGURE 11. The population-mean distance, $\langle D \rangle_\pm(t)$, between pairs of nearest neighbour vortices, segregated by whether the pair is like-sign (dot-dashed and solid lines) or opposite-sign (dashed and dotted lines) in the q extrema. The distance is measured between the nearest vortex-element extrema in separate compound vortices.

as they would be if the vortices were uniformly distributed on a lattice, $D_0 = 2\pi n_{cv}^{-1/3}$ and even a little less than half as large as the average nearest neighbour distance for completely random distribution, $\langle D_r \rangle \approx 1.1\pi n_{cv}^{-1/3}$ (see Appendix B). This indicates that the nearby vortices are usually closer together than would occur with uniform or random positioning.

We next examine the global ordering among vortices by constructing a lag-correlation function among the compound vortex centers. We define this as

$$C(r,z) = \overline{s_i q_{cv_i} s_j q_{cv_j}} \Big|_{|\boldsymbol{x}_i - \boldsymbol{x}_j| \approx \sqrt{r^2 + z^2}} \Big/ \langle q_{v_i}^2 \rangle, \tag{14}$$

where $s_i = \pm 1$ is the sign of the q_{cv} extremum in vortex i, the overbar denotes an average over all vortex pairs whose horizontal and vertical separation distances are r and z, and the angle brackets denote an unconditional average over the vortex population. The sampling requirements on estimating C accurately are rather severe, since it requires there be many vortex pairs with separation distances close to each (r,z). In practice we choose to bin the separation distances with a somewhat large bin size of $\Delta r = \Delta z = 0.2$ for calculating the conditional averages in (14). However, even with large bins estimates of $C(r,z)$ are somewhat noisy. Therefore, we shall measure the global positional ordering by an appropriate integral moment of C, defined below. Our goal is to measure the degree that like-sign vortices cluster in configurations that are approximately aligned in the vertical.

During the period shortly after vortex emergence, $C(r,z)$ is indistinguishable from zero at all non-zero spatial lags. Over time an ordering develops that is qualitatively similar to the one indicated by the near-neighbour angle distributions: $C > 0$ for $z > r$ and $C < 0$ for $r > z$. This ordering starts initially at small lag distances, $D = \sqrt{r^2 + z^2}$, and extends further outward with further evolution. We define an

integral moment to measure this behaviour in $C(r, z)$ by

$$\mathscr{I}_C = \int_0^{r_{max}} \int_0^{z_{max}} C(r, z) F(\theta(r, z)) \, \mathrm{d}r \, \mathrm{d}z, \qquad (15)$$

and its time history is plotted in figure 12. As above, $\theta = \tan^{-1}[r/z]$ is the positive angle of the separation vector away from the horizontal plane (as in (12)). We evaluate (15) by discrete quadrature and choose $r_{max} = z_{max} = 2.0$. To accomplish the measurement of clustering behaviour, the function $F(\theta)$ is negative for like-sign vortex separations that are mostly horizontal and positive for ones that are mostly vertical. Thus the positive magnitude of $\mathscr{I}_C$ is a measure of the degree of the global ordering described above. A simple choice for F with this character is the function $F(\theta) = -\cos 2\theta$. A similar but somewhat better choice is one based on the most probable angle for random vortex distributions, θ_0 from (13). The desired function mimics the properties of $F(\theta) = -\cos 2\theta$ except for being centred about θ_0. We choose a piecewise cubic spline that has values and derivatives at $\theta = 0$, θ_0, and $\pi/2$ of

$$F(\theta) = \begin{cases} -1, & \theta = 0 \\ 0, & \theta = \theta_0 \\ +1, & \theta = \pi/2 \end{cases} \qquad F'(\theta) = \begin{cases} 0, & \theta = 0 \\ 1, & \theta = \theta_0 \\ 0, & \theta = \pi/2. \end{cases}$$

This function is

$$F = \begin{cases} -1 + \theta(\theta - \theta_0)/\theta_0, & 0 \leqslant \theta \leqslant \theta_0 \\ (\theta - \theta_0) + (\theta - \theta_0)^2 - (\theta - \theta_0)^3, & \theta_0 \leqslant \theta \leqslant \pi/2. \end{cases} \qquad (16)$$

The resulting $\mathscr{I}_C(t)$ is shown in figure 12. Its early value is essentially zero, indicating a lack of global ordering among vortex positions, but later it becomes increasingly positive, indicating the development of clustering. A very similar result is obtained with the alternative function $F = -\cos 2\theta$, indicating that the choice of an integral weighting function is not a particularly sensitive one. Positive values of $\mathscr{I}_C$ begin to develop after about $t = 15$. This is later than the appearance of near-neighbour angle differences (figure 10), and it indicates that the global ordering among vortices evolves out of the prior pairwise ordering. The value of $\mathscr{I}_C$ continues to increase as the solution approaches the end-state configuration of two fractured columns of like-sign vortices.

6. Discussion

Our vortex census demonstrates some of the important properties of coherent vortices in decaying geostrophic turbulence. Through non-conservative interactions among close vortices, the population evolves towards fewer, larger, and sparser vortices. We find statistical evidence that is consistent with the importance of the aggregation processes of merger and alignment between like-sign vortices: horizontal and vertical size growth, vertical clustering, and a late-time approach to the non-turbulent end state of two aligned, like-sign columns of vortices. We also find that there is a regime of approximately self-similar temporal evolution in the vortex statistics (i.e. with power-law functional forms) during a somewhat brief interval that starts after an earlier period where small, weak vortices are more likely to be destroyed and ends before the approach to the end state. Furthermore, we present a mean-vortex scaling theory based on the conservation of energy, vortex extremum, and vortex aspect ratio. Its predictions are approximately consistent with the measured ratios among the power-law exponents for vortex properties, albeit with modest discrepancies that
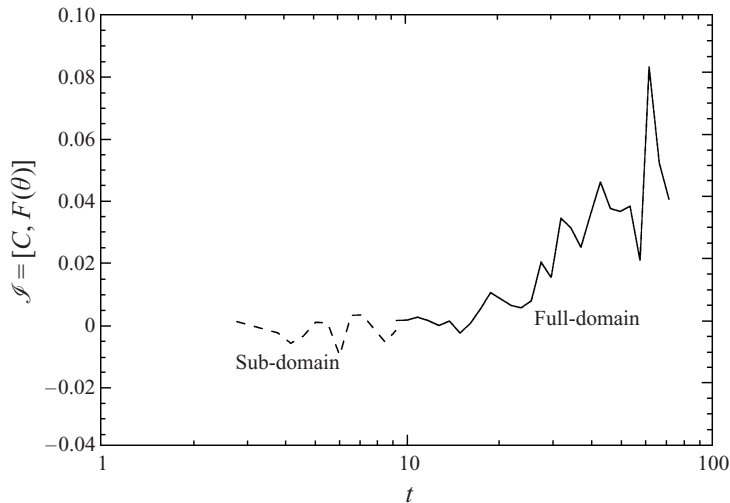
FIGURE 12. Covariance time series, $\mathcal{I}_C$, between $C(r, z, t)$ and $F(\theta)$ as defined in (15)–(16). Positive values indicate vertical clustering among like-sign vortices.

are plausibly due to a greater enstrophy dissipation rate in our solutions than might occur with a larger value for Re. Because of the limited size of both Re and the vortex population size, we cannot assess the scaling hypotheses with great certainty.

Despite the uncertainties in our results there is a strong likelihood that we have seen a glimpse of the generic high-Re behaviour for at least a class of initial conditions with a narrow-band spectrum. In scouting for the MWY94 solution, we examined solutions on coarser grids, with different initial conditions and dissipation operators, and at lower Re; in all cases the phenomenology was similar to what we have reported here. If we were able to calculate a solution with extremely high Re, a narrow-band initial condition would be well separated from both the domain scale and the dissipation scale. Here, the grid resolution allows only a single order of magnitude to separate the initial flow scale and each of the other two scales. It seems plausible that this is sufficient to see the beginnings of high-Re behaviour. But this is still a somewhat modest realization of this asymptotic limit, and the temporal scaling behaviour might be more unambiguous at higher Re. In two-dimensional turbulence, temporal scaling behaviour was first identified at Re values close to the present one, and later it was confirmed at much higher Re (Bracco *et al.* 1999).

From the analogy with two-dimensional turbulence, we would not be surprised if broad-band initial conditions gave rise to spatial scaling behaviour, at least for some time interval, rather than the temporal scaling seen here (Santangelo, Benzi & Legras 1989; Weiss 1999; Bracco *et al.* 1999). Thus, the temporal scaling behaviour applies to turbulent flows in which random perturbations inject enstrophy into the fluid with a well-defined length scale, as could occur in a mean-flow instability process. We have not yet examined solutions for forced, equilibrium geostrophic turbulence, at least in part because of our uncertainty about how to choose the forcing in a physically relevant way. Our expectation is that coherent vortices could play a significant role in this regime, at least on scales as large or larger than the forcing scale (cf. Borue 1994). On the other hand, we also expect important differences in vortex and turbulence dynamics on planetary scales due to a small domain aspect ratio and spatial variations in f and N.

The interaction dynamics among geostrophic vortices are not yet very well understood, but we can infer some additional information about their outcomes from the census report. The vortex population number decays much faster for geostrophic vortices than for two-dimensional vortices, consistent with a faster enstrophy decay rate. This implies that the three-dimensional processes that amalgamate or destroy geostrophic vortices are more efficient than in two dimensions. We find that an alignment event among close vortices is not often carried to a complete amalgamation, since relatively few compound vortices develop that are composed of more than a single vortex element and the average separation angle among nearest like-sign neighbours remains well below $\pi/2$. This is consistent with the existence of a hole in the pair-alignment critical separation curve for a radial separation distance that is small compared to the vertical one (Sutyrin *et al.* 1998), as well as the persistence of non-aligned wave-like motions within clusters (Clyne *et al.* 1998). Therefore, either straining destruction of nearby vortices (without amalgamation) or merger between vortices with a relatively small vertical separation between their core extrema, or both, must occur with a greater frequency in geostrophic turbulence than do mergers in two-dimensional turbulence. Nevertheless, at least a tendency towards alignment is evidently the result of some important interaction process, since strong vertical clustering develops and eventually leads to a global organization of the surviving vortices into the non-turbulent, columnar end state. Another inference is that a preferred vortex aspect ratio is strongly selected during vortex interactions, causing the vortices to have a shape that is a distorted form of Charney isotropy: the mean aspect ratio is $a = 0.83$ in stretched coordinates, and the equivalent Burger number based on physical coordinates, $B = (Nh/fR)^2$, is 0.7. Barotropic and baroclinic instabilities in QG dynamics might be invoked broadly to preclude particularly large and small values of B, respectively, but this does not seem a sufficient explanation for the very small B variations we measure here. This argument is even stronger insofar as the elemental vortex shape is a q-monopole that is linearly stable for any value of B. Thus, we infer that the non-conservative relaxation of an initially deformed vortex towards the ideal axisymmetric, aligned, stationary configuration must involve q filamentation that efficiently moves B towards its preferred value (e.g. as during the late stages of vortex merger; von Hardenberg *et al.* 1999). Finally, we have noticed in viewing animations that close, multi-vortex interactions are frequent and often persistent, to a much greater degree than in two-dimensional turbulence. Therefore, we suspect that the population evolution cannot be explained entirely in terms of pair interactions alone, hence some reconsideration is warranted for the conceptual picture that coherent vortices are usually well separated from each other except for rare, brief, dissipative, pairwise close encounters.

The descriptive nature of this census report indicates that there remain significant open questions about the interaction dynamics among three-dimensional, QG coherent vortices. We believe they can, and should, be addressed in idealized initial-value problems. Our hope is that a systematic understanding of vortex dynamics will provide the basis for a conceptual and computationally realizable theory for homogeneous geostrophic turbulence.

Appendix A. The MWY94 solution

The equations (2)–(6) are solved in non-dimensional form in the stretched isotropic coordinates defined preceding (7). The computational domain is $[0, 2\pi]^3$, with periodic boundary conditions in all directions. The dynamical evolution is unforced, and the form we choose for the dissipative operator in (2) is biharmonic hyperdiffusion, namely

$$\mathcal{NCT} = -\nu\nabla^4 q. \tag{A 1}$$

This is a three-dimensional Charney-isotropic operator that implies that both $\mathscr{E}$ and $\mathscr{Z}$ be non-decreasing in (2) (i.e. in the absence of computational errors), although it does not assure that isolated q extrema are non-increasing for non-smooth fields (unlike Newtonian diffusion). The hyperviscous coefficient is chosen as $\nu = 1.14 \times 10^{-8}$, which is as small as is consistent with at least marginally smooth solutions on the grid.

The choice of a hyperdiffusion operator is motivated by the desire to have a weaker dissipation on a given computational grid than occurs with Newtonian diffusion. While the effects of this choice have not been systematically investigated in QG turbulence, they have been explored extensively in two-dimensional turbulence and other fluid dynamical regimes. On the basis of this experience, we may reasonably assume that the results of this paper are not strongly influenced by the choice of dissipation operator. Our understanding of turbulent cascades is that the details of enstrophy removal in the dissipation range do not greatly affect the larger scales, especially where an inverse cascade occurs. The form of the sub-grid-scale parameterization of dissipation in two-dimensional turbulence does not impede the self-organization into coherent vortices and their merger interactions, although it can affect the profile of the vortex cores at late times (Shchepetkin & McWilliams 1998). But since the population dynamics is largely governed by mutual advection of separated vortices these profile differences should not be very important in determining the population statistics, except in ways that can be generally understood as a *Re* dependence (see §6).

The initial conditions are a random-phase realization of a narrow-band, Charney-isotropic spectrum peaked at $\kappa_0 = 22.0$, with a normalization such that the initial energy, $\mathscr{E}$, is unity. The grid size is $N^3 = 320^3$, and the integration spans $t = 0$–72. The computational method is described in Yavneh & McWilliams (1996). It uses second-order, centred, finite-difference operators in space and time for (1), (7), and (A 1). The advection operator is represented as an Arakawa Jacobian. The time-stepping method is fully implicit using a Multigrid Full Approximation Scheme iterative solver with partial coarsening (i.e. there is a grid hierarchy in x_h but not z). Moderate computational noise is evident at early time in non-monotonic behaviour of q extrema, due primarily to dispersive advection errors in the vicinity of sharp q gradients (rather than as a direct consequence of the hyperdiffusion operator) that are insufficiently damped by the small ν value used; after a time of ~ 1 (i.e. before the vortex-dominated regime of interest here), this noise behaviour becomes quite weak.

The time of the largest $\mathscr{Z}$ dissipation rate is $t \approx 1$, which is about 10 times the initial eddy turnover time, $2\pi\mathscr{Z}^{-1/2}$. The total decay in $\mathscr{E}$ is only 3% over the integration, whereas the decay in $\mathscr{Z}$ is nearly 99%. The kurtosis of q, a measure of spatial intermittency, grows from its initial Gaussian value of ≈ 3 to more than 100. The isotropic wavenumber spectrum $\mathscr{E}(\kappa)$ is initially quite narrow. Its peak wavenumber moves progressively to smaller κ. The spectrum shape for intermediate κ approaches the enstrophy inertial-range form, $\sim \kappa^{-3}$, around the time of maximum enstrophy dissipation, but thereafter it steepens with time.

Appendix B. Nearest neighbour separation among random vortices

We derive $\langle D_r \rangle$, the expected near-neighbour separation distance, for n_{cv} point vortices distributed randomly in a triply-periodic cube of side L in the high-density limit: $n_{cv} \gg 1$. The vortices are assumed to be distributed independently with uniform random distribution.

Fix a single vortex i at the domain centre. (Due to the periodicity, any vortex can be considered as being at the centre.) Consider some $r \leqslant L/2$. The probability that any particular point vortex is at a distance smaller than r from vortex i is equal to the ratio of the volume of the ball of radius r to the volume of the domain: $\frac{4}{3}\pi r^3 / L^3$. Hence, the probability that n_{cv} vortices are all at a distance *greater* than r from vortex i is

$$F(r) = \left(1 - \tfrac{4}{3}\pi r^3 / L^3\right)^{n_{cv}}.$$

The probability that D_i – the distance from vortex i to its nearest neighbour – is between r and $r + \Delta r$ is evidently $F(r) - F(r + \Delta r)$. Taking the limit $\Delta r \to 0$, we find the density function for D_i to be

$$f(r) = -F'(r).$$

The expected value for the distance to the nearest neighbour is given by

$$\langle D \rangle = \int_0^{L/2} r f(r)\, \mathrm{d}r = \frac{L}{2} F\left(\frac{L}{2}\right) + \int_0^{L/2} F(r)\, \mathrm{d}r,$$

where we have employed integration by parts. Here we have neglected the probability that the nearest neighbour is located outside the ball of radius $L/2$, but this probability is $\sim \exp(-n_{cv})$, so it is negligible for large n_{cv}. For the same reason we can now neglect $L/2\, F(L/2)$. Introducing the variable change

$$\hat{r} = \left(\tfrac{4}{3}\pi n_{cv}\right)^{1/3} \frac{r}{L},$$

we obtain

$$\langle D \rangle = L \left(\tfrac{4}{3}\pi n_{cv}\right)^{-1/3} \int_0^{1/2\left(\frac{4\pi n_{cv}}{3}\right)^{1/3}} \left(1 - \hat{r}^3/n_{cv}\right)^{n_{cv}} \mathrm{d}\hat{r}.$$

In the limit $n_{cv} \to \infty$ the integral tends to

$$\int_0^\infty \exp\left(-\hat{r}^3\right) \mathrm{d}\hat{r} = \Gamma(4/3).$$

This yields

$$\langle D \rangle = L \left(\tfrac{4}{3}\pi n_{cv}\right)^{-1/3} \Gamma(4/3) \approx 0.554 L n_{cv}^{-1/3}.$$

Thus, the expected distance between nearest neighbours is a factor of 0.554 its value if the vortices are distributed uniformly on a lattice. This value was matched well in computational simulations with several hundreds or thousands of randomly distributed points.

REFERENCES

ARAKAWA, A. & SCHUBERT, W. H. 1974 Interaction of a cumulus cloud ensemble with a large-scale environment. Part I. *J. Atmos. Sci.* **31**, 674–701.

BENZI, R., PATERNELLO, S. & SANTANGELO, P. 1986 On the statistical properties of decaying turbulence. *Europhys. Lett.* **3**, 811–818.

BENZI, R., COLELLA, M., BRISCOLINI, M. & SANTANGELO, P. 1992 A simple point-vortex model for two-dimensional decaying turbulence. *Phys. Fluids* A **4**, 1036–1039.

BOER, G. J. & SHEPHERD, T. G. 1983 Large-scale two-dimensional turbulence in the atmosphere. *J. Atmos. Sci.* **40**, 164–184.

BORUE, V. 1994 Inverse energy cascade in stationary two-dimensional homogeneous turbulence. *Phys. Rev. Lett.* **72**, 1475–1478.

BRACCO A., MURANTE, G., PROVENZALE, A. P., MCWILLIAMS, J. C. & WEISS, J. B. 1999 Revisiting two-dimensional turbulence at modern resolution. Preprint.

CARNEVALE, G. F., MCWILLIAMS, J. C., POMEAU, Y., WEISS, J. B. & YOUNG, W. R. 1991 Evolution of vortex statistics in two-dimensional turbulence. *Phys. Rev. Lett.* **66**, 2735–2737.

CHARNEY, J. 1971 Geostrophic turbulence. *J. Atmos. Sci.* **28**, 1087–1095.

CHORIN, A. J. 1994 *Vorticity and Turbulence*. Springer.

CLYNE, J., SCHEITLIN, T. & WEISS, J. B. 1998 Volume visualizing high-resolution turbulence computations. *Theor. Comput. Fluid Dyn.* **11**, 195–211.

DRITSCHEL, D. G., TORRE JUÁREZ, M. DE LA & AMBAUM, M. H. P. 1999 The three-dimensional vortical nature of atmospheric and oceanic turbulent flows. *Phys. Fluids* **11**, 1512–1520.

FARGE, M. & PHILIPOVITCH, T. 1993 Coherent structure analysis and extraction using wavelets. In *Progress in Wavelet Analysis and Applications* (ed. Y. Meyer & S. Roques), pp. 477–481. Editions Frontières, Paris.

FU, L.-L. 1983 On the wavenumber spectrum of oceanic mesoscale variability observed by the SEASAT altimeter. *J. Geophys. Res.* **88**, 4331–4341.

HERRING, J. 1980 Statistical theory of quasigeostrophic turbulence. *J. Atmos. Sci.* **37**, 969–977.

HARDENBERG, J. VON, MCWILLIAMS, J. C., PROVENZALE, A., SHCHEPETKIN, A. & WEISS, J. B. 1999 Vortex merging in quasigeostrophic flows. *J. Fluid Mech.* (submitted).

HUA, B. L. & HAIDVOGEL, D. B. 1986 Numerical simulations of the vertical structure of quasi-geostrophic turbulence. *J. Atmos. Sci.* **43**, 2923–2936.

HUA, B. L. & KLEIN, P. 1998 An exact criterion for the stirring properties of nearly two-dimensional turbulence. *Physica* D **113**, 98–100.

HUA, B. L., MCWILLIAMS, J. C. & P. KLEIN, P. 1998 Lagrangian acceleration and dispersion in geostrophic turbulence. *J. Fluid Mech.* **386**, 87–108.

JEONG, J. & HUSSAIN, F. 1995 On the identification of a vortex. *J. Fluid Mech.* **285**, 69–94.

MCWILLIAMS, J. C. 1989 Statistical properties of decaying geostrophic turbulence. *J. Fluid Mech.* **198**, 361–385.

MCWILLIAMS, J. C. 1990a The vortices of two-dimensional turbulence. *J. Fluid Mech.* **219**, 361–385.

MCWILLIAMS, J. C. 1990b The vortices of geostrophic turbulence. *J. Fluid Mech.* **219**, 387–404.

MCWILLIAMS, J. C., WEISS, J. B. & YAVNEH, I. 1994 Anisotropy and coherent vortex structures in planetary turbulence. *Science* **264**, 410–413 (referred to herein as MWY94).

METAIS, O., RILEY, J. J. & LESIEUR, M. 1994 Numerical simulations of stably stratified rotating turbulence. In *Stably Stratified Flows: Flow and Dispersion over Topography* (ed. I. P. Castro & M. J. Rockwell), pp. 139–151. Clarendon.

METAIS, O., BARTELLO, P., GARNIER, E., RILEY, J. J. & LESIEUR, M. 1996 Inverse cascade in stably stratified rotating turbulence. *Dyn. Atmos. Oceans* **23**, 193–203.

NASTROM, G. D. & GAGE, K. S. 1985 A climatology of atmospheric wavenumber spectra of wind and temperature observed by commercial aircraft. *J. Atmos. Sci.* **42**, 950–960.

OHKITANI, K. 1991 Wavenumber space dynamics of enstrophy cascade in a forced two-dimensional turbulence. *Phys. Fluids* A **3**, 1598–1611.

POLVANI, L. M. 1991 Two-layer geostrophic dynamics. Part 2. Alignment and two-layer V-states. *J. Fluid Mech.* **225**, 241–270.

RHINES, P. B. 1979 Geostrophic turbulence. *Ann. Rev. Fluid Mech.* **11**, 401–411.

RICCARDI, G., PIVA, R. & BENZI, R. 1995 A physical model for merging in two-dimensional decaying turbulence. *Phys. Fluids* **7**, 3091–3104.

SALMON, R. 1982 Geostrophic turbulence. *Topics in Ocean Physics, LXXX Corso'*, pp. 30–78. Soc. Italiana di Fisica, Bologna.

SANTANGELO P., BENZI, R. & LEGRAS, B. 1989 The generation of vortices in high-resolution two-dimensional decaying turbulence and the influence of initial conditions on the breaking of self-similarity. *Phys. Fluids* A **1**, 1027–1034.

SHCHEPETKIN, A. & MCWILLIAMS, J. C. 1998 Quasi-monotone advection schemes based on explicit locally adaptive dissipation. *Mon. Weath. Rev.* **126**, 1541–1580.

SIEGEL, A. & WEISS, J. B. 1997 A wavelet-packet census algorithm for calculating vortex statistics. *Phys. Fluids* **9**, 1988–1999.

STAMMER, D. 1997 Regional characteristics of ocean variability estimated from global TOPEX/POSEIDON altimeter measurements. *J. Phys. Oceanogr.* **27**, 1743–1769.

SUTYRIN, G. G., MCWILLIAMS, J. C. & SARAVANAN, R. 1998 Co-rotating stationary states and vertical alignment of geostrophic vortices with thin cores. *J. Fluid Mech.* **357**, 321–349.

VERRON, J., HOPFINGER, E. & MCWILLIAMS, J. C. 1990 Sensitivity to initial conditions in the merging of two-layer baroclinic vortices. *Phys. Fluids* A **2**, 886–889.

VIERA, F. 1995 On the alignment and axisymmetrization of a vertically tilted geostrophic vortex. *J. Fluid Mech.* **289**, 29–50.

WEISS, J. 1991 The dynamics of enstrophy transfer in two-dimensional hydrodynamics. *Physica* D **48**, 273–294.

WEISS, J. B. & MCWILLIAMS, J. C. 1993 Temporal scaling behaviour of decaying two-dimensional turbulence. *Phys. Fluids* A **5**, 608–621.

WEISS, J. B. 1999 Punctuated Hamiltonian models of structured turbulence. In *Semi-Analytic Methods for the Navier–Stokes Equations (Montreal, Canada, 1995)* (ed. K. Coughlin). CRM Proc. Lecture Notes, Vol. 20, pp. 109–119. Am. Math. Soc., Providence, RI (in press).

YAVNEH, I. & MCWILLIAMS, J. C. 1996 Multigrid solution of stably stratified flows: the quasi-geostrophic equations. *J. Sci. Comput.* **11**, 47–69.